Author's Accepted Manuscript

A functional assembly of SiO$_2$ nanospheres/ Graphene oxide composites

J. Iturbe-Ek, J. Andrade-Martínez, R. Gómez, V. Rodríguez-González

www.elsevier.com/locate/matlet

Cite this article as: J. Iturbe-Ek, J. Andrade-Martínez, R. Gómez, V. Rodríguez-González, A functional assembly of SiO$_2$ nanospheres/Graphene oxide composites, *Materials Letters,* http://dx.doi.org/10.1016/j.matlet.2014.11.149

A functional assembly of SiO₂ nanospheres/Graphene Oxide composites

J. Iturbe-Ek,[1] J. Andrade-Martínez[1,2], R. Gómez[3] and V. Rodríguez-González[1,]*

[1]*División de* Materiales *Avanzados, Instituto Potosino de Investigación Científica y Tecnológica, San Luis Potosí, S.L.P., México.*

[2]*Doctorado Institucional en Ingeniería y Ciencia de Materiales, Universidad Autónoma de San Luis Potosí, SLP, México*

[3]*Universidad Autónoma Metropolitana-Iztapalapa, Departamento de Química, ECOCATAL, México, D. F., México*

corresponding author email: vicente.rdz@ipicyt.edu.mx; Tel: +52 44483 42000 ext. 7295

Abstract

A novel assembly of SiO₂ nanospheres functionalized on graphene oxide (GO) sheets was prepared by the one-step microwave-hydrothermal method. The nanocomposites were well characterized and investigated to study their Rhodamine B (RhB) adsorption capacity and their RhB reduction activity using hydrazine as a sacrificial electron donor. The SiO₂-GO-*RhB* composites showed fluorescent properties.

Keywords: GO nanocomposites; SiO₂ nanospheres, adsorptive capacity, fluorescent properties, RhB reduction.

1. Introduction

The development of graphene-oxide-based nanocomposites was prompted by some detrimental disadvantages displayed by GO such as stability, adsorption capacity, structural layer defects, water dispersibility, low photoactivity and aggregation among others [1-4]. Adsorption capacity and photocatalytic removal of dyes by using graphene or GO have been the topics of some recent publications [5-7]. GO nanocomposites were scarcely used with this purpose; selective adsorption, agglomeration or stability have been taken into account for comparative adsorptive studies versus carbon materials such as carbon nanotubes (CNTs) and GO [8]. Nanocomposite-based carbon materials are another good option for the adsorption of hazardous dyes and the combination with mesoporous materials could extend their applications as ion adsorption agents, energy storage sensors and fluorescent materials [9-15].

GO-based SiO_2 nanocomposites are the subject of the present research. We presented a detailed study of the characterization of an assembly of mesoporous SiO_2 nanospheres on GO, its use in Rhodamine B (RhB) adsorption-reduction processes and its subsequent recovery are discussed herein.

2. Experimental

GO was obtained by the improved Hummers method [16], which consists in one-hydrothermal exfoliation step and reduction in a microwave oven, (See electronic Supplementary Information, SI). The obtained GO was used for the SiO_2 nanospheres/GO funcionalization [17]. Previously, mesoporous SiO_2 was obtained by the modified Stöber method, using cetyltrimethylammonium bromide (CTAB, Aldrich 99%) to control the morphology and mesoporosity [18-19]. The resulting assembly was labeled as GO-SNS, where GO denotes graphene oxide and SNS denotes SiO_2 nanospheres. Details of the synthesis are included in Supplementary Information.

3. Results and discussion

XRD patterns of bare materials and composites are shown in Fig. 1a. The broad diffraction peaks at 2 *theta*= 12.2°, 25.2° and 43.4° in the GO pattern suggest the expansion and exfoliation of graphite in a few GO layers and could be indexed to the GO [JCPDS 25-284]. Normally, the exfoliation of layers develops in a turbostatic way, and the estimation of the interplanar spacing between layers was $d_{(002)}$= 8.5 Å. For the SNS, the maximum a broad XRD peak at 2 *theta* = 15 to 30° matches well with the SiO$_2$ spheres [Cristobalite, JCPDS 29-0085] synthesized by the modified Stöber method [20].

The GO FTIR spectra show the functional groups over the GO layers resulting from the oxidation of graphite, Fig. 1b. Notably, the GO bands at 1553 (C=C), 1364 (OH$^-$ species) and 918.5 cm^{-1} (O-C–O stretching), in addition to the band of the SNS spheres at 983 cm^{-1} for silanol groups [21-22] diminish their intensity and were slowly blue shifted when the SNS were grafted onto GO. The most intense band at 1071 cm^{-1}, ascribed to the v_{as} stretching of Si-O-Si [23], was decreased when the SNS were incorporated onto the GO surface layers. The band at 925 cm^{-1} for GO-SNS corresponds probably to Si-O-C bonding vibrations resulting from a combination of the 918.5 cm^{-1} (O-C–O) bond of GO and Si-O-Si bond of SNS. Silanol groups allow the anchorage of the spheres on sp^2-sp^3 GO defects [17], prompting the successful assembly of SiO$_2$ and GO into GO-SNS.

The mesoporosity of the SNS was evaluated by N$_2$ physisorption as shown in Fig. 1c. The SNS show a typical adsorption-desorption isotherm featured by mesoporous materials (Type IV) with a thin hysteresis loop that occurs at relative pressures of 0.15 to 0.3 due to some microporosity; another branch from 0.81 to 0.98 P/P$_0$ corresponds mainly to the intersphere voids; the surface specific area, (A$_{BET}$), was 993.51m^2/g. In the case of the GO, the isotherms are of Type I with classical behavior for layered materials, featuring a large hysteresis loop from 0.4 to 0.8, which indicates the presence of microporosity, mesoporosity, and some macroporosity [25], confirming the turbostatic GO arrangement with wrinkled morphology. The GO sheets show only 65.8m^2/g of A$_{BET}$, mainly due to the space between corrugated layers. The GO-SNS assembly also shows

hysteresis Type IV and isotherms with a hysteresis loop that is typical of mesoporous SiO_2 spheres filled totally at high relative pressure, which are between the GO layers. As for the assembly of SNS onto the few GO layers, they are assumed to contain connected pore networks between particle and layer voids, thus the hysteresis from 0.6 to 0.93 is of Type H_2, which represents a homogenous distribution of SNS all over the GO layers in conjunction with the hexagonal arrangement of mesopores of SNS. Analogous mesoporous attribution of textural properties was reported for GO–Fe_3O_4 nanocomposites structures where the loading of GO tailors the pore structure of the nanocomposites [26]. The pore size distributions from 2 to 30nm corresponds to the interparticle voids (Fig. 1d); the A_{BET} of 192.7m^2/g is comparable with that featured by other GO composites [27]. Pore size distributions confirm the wrinkled morphology of the GO, indicating occlusion of the pores covered by the GO layers in GO-SNS. The pore size distribution of the SNS presents a maximum at 2.4 nm and a A_{BET} of 993.5 m^2/g [21]. The surface of the SNS consists of Si-OH and some Si-O-Si bridges, which serve as attaching groups to GO layers. GO, which is mainly positively charged [7, 24] favors the functionalization of the negatively charged SNS [23], according to the isoelectric points reported for SiO_2 adsorbents [23]. The BET-BJH model was used because it takes into account a multilayer formation and provides more insights about corrugation of turbostatic GO layers in conjugation with the SNS spheres functionalization. Nevertheless, the T-plot method seems more appropriate for evaluating the external surface of the microporosity of corrugated GO (see Figure S1 in SI) and further characterization will be carried out in order to understand the new hybrid structure of GO-SNS microporosity.

The TEM images display the SNS size of 100 nm on average, Fig 2d, well dispersed over the GO layers without notable agglomerations, Figs. 2a-2b. No preferential sites were observed for grafted SNS. In Fig 2b, it is possible to distinguish the mesoporosity of the SNS over the layers of GO sheets with wrinkled morphology. The mesoporosity of the SNS was confirmed by a HRTEM image, Fig. 2c. It clearly shows the hexagonally ordered mesoporosity of SNS. The SNS allow the stabilization and restoration of the GO layers, forming GO-SNS composites.

For testing the effect of SiO_2 spheres on the adsorptive capacity of the GO-SNS composites, the recalcitrant RhB dye was used as an adsorbate. Figures 3 a)-b) show the adsorption experiments as functions of time, for 5 and 10 ppm of RhB. The rapid RhB adsorption was stabilized in almost 30 min for both GO and SNS. This behavior was supposed to occur on functional oxygen groups and π-π GO domains [17] due to the mesoporosity, silanol and siloxane groups and the high A_{BET} of the SNS [18, 19]. RhB is trapped into the pores volume of SNS [23]. The GO-SNS composite achieved the adsorption equilibrium in 60 min, while most of the bare GO and SNS reached the adsorption plateau after 90 min. In Fig. 3b, it can be also observed that by controlling the composite quantity, the total adsorption is delayed by more than 90 min. In Fig. 3a, the adsorption capacity was obtained up to 50, 100 and 200 mg of GO-SNS, see Table S1 in SI. As the amount of GO-SNS is increased, the equilibrium is more rapidly achieved. More than 5 ppm of RhB starts to saturate the SNS adsorption sites. The isotherm results were fitted with the Langmuir model. It has been reported that the RhB adsorption on mixed oxides best fits Langmuir, in contrast with other isotherm models [23-24]. The resulting adsorptive capacities are important, although not comparable with sorbates like pillared clays, flue-ash or activated carbon. The RhB adsorption in water exhibited a strong adsorption capacity of 40 mg g^{-1} with a contact time of 30 min.

In order to evaluate the stability and the reversibility of the RhB adsorption, the GO-SNS nanocomposite was recovered after the adsorption experiments and introduced in 100 mL of water, under strong stirring for 15 min, as a washing system. Then, the solution was filtered by using a hydrophobic filter and finally, the solution was monitored by UV-vis spectroscopy to check if RhB dissolves again in water. No apparent dissolution was observed during the washing process. RhB is strongly adsorbed on GO-SNS. Only SNS took the color of RhB while GO-SNS conserve its black color. According to the Langmuir model, the RhB molecules are adsorbed on a monolayer in a different equivalent site on the surface, which means equivalent sites either on the SNS or GO

surface. It has been reported that RhB is adsorbed in a dimer form ($^{+}N(C_2H_5)_2$) on the negative surface of the SiO_2 and also trapped in the pore volume [23, 24].

The influence of the UV-irradiation on the electron-donating abilities of the GO-SNS was explored, see details in SI: (**i**) UV-irradiation experiments were carried out by using a 365 or 254 nm pen-ray UV-lamp, but the UV photo-oxidation resulted in a negligible process. The photocatalytic decomposition of RhB was not possible due to the strong and irreversible adsorption of RhB; besides, SiO_2 is not a semiconductor and the molecules are attached to the sp^2-sp^3 defect domains and by the functional oxygen groups of GO. We have already stated that adsorption governs the RhB photodegradation by using AgNPs-GO composites [7]. (**ii**) The use of hydrazine as a sacrificial electron donor during UV-irradiation allows the 50% of RhB reductive degradation, Fig. 3c. First, the RhB degradation in presence of hydrazine only is negligible; RhB seems to be resistant to the reductive attack of hydrazine. Secondly, we noticed that if 365nm UV-irradiation were added to the reduction, the degradation increased to 55%, while by using 254nm UV, degradation reached 70%, mainly due to the photolysis of RhB.

The electron transfer from hydrazine to RhB was mediated by GO-SNS assembly. When hydrazine was added to the slurry, the electron transfer reaction started. N_2H_4 in aqueous medium produces $[N_2H_5]^{+}$ and OH^{-} ions, which can reduce and oxidize the RhB. However, the cleavage of RhB over GO surface contends with the degradation rate. The reuse of recovered GO-SNS and SNS was performed in a second cycle of RhB adsorption (10 ppm), but a negligible RhB adsorption was observed. The adsorption sites seem to be saturated in the first adsorption step. UV-vis spectra of the GO-SNS before and after RhB adsorption and after UV-irradiation are shown in Fig. 3d. An adsorption band from 450 to 600 nm for SNS showing RhB adsorption can be observed and there may be fluorescence sensitization by RhB, chromophore cleavage [23]. In the case of the GO-SNS composites, the weak adsorption signal is manifested from 500 to 600 nm (50 ppm). Based on

6

earlier reports that GO in aqueous medium can show florescence in the visible range due to the functional oxidized carbon groups [28]. In our case, RhB substitutes oxidized carbon groups in GO edges and acts electron-transfer fluorescence quencher [29]. RhB then injects electrons to reduce GO layers suppressing photoactivity and diminishes fluorescence emission [7-30].

This immobilization technique of well-prepared SiO_2 nanospheres on a GO substrate looks more practical than other techniques such as spray coating, sputtering, sol-gel method, evaporation induced self-assembly and the ultrasonic spray pyrolysis method [25]. Besides, the immobilization does not require the use of grafting agents such as 3-aminopropyl triethoxysilane (APTES) or other silane agents [31]. GO-SNS nanocomposites could have potential use in biotechnological applications such as dye tracers, dye identification tests, bio markers, and the SNS use as high-visibility textile products [31], sensors and markers based on thin films [32, 33].

4. Conclusions

GO-SNS nanocomposites were synthesized by a hydrothermal technique, which produces highly dispersed SiO_2 nanospheres onto GO layers. These novel composites may offer advantages such as removal of dyes from aqueous environments. Irreversibility tests demonstrated a strong adsorption capacity with more than 99% of RhB removal, which was fitted with the Langmuir model.

The reduction activity using hydrazine as a sacrificial electron-donor allowed a 50% degradation of 5 ppm of RhB in 2 hours. The recovered SNS mesoporous material presented fluorescent RhB properties that can be used in high visibility paint products.

Electronic Supplementary Information (SI) available: [Detailed Synthesis of GO-SNS composites, photoassisted, Table S1 with adsorption parameters and pore size distribution: micropores (Horwath Kawazoe)].

References

1   Paredes JI, Villar-Rodil S, Martínez-Alonso A, Tascón JMD. Graphene Oxide Dispersions in Organic Solvents, Langmuir 2008;24:10560-4.
2   Dreyer DR, Park S, Bielawski CW, Ruoff RS. The chemistry of graphene oxide. Chem. Soc Rev 2010;39:228-40.
3   Erickson K, Erni R, Lee Z, Alem N, Gannett W, Zettl A. Determination of the Local Chemical Structure of Graphene Oxide and Reduced Graphene Oxide. Adv Mater 2010;22:4467-72.
4   Taherian F, Marcon V, van der Vegt NFA, Leroy F. What Is the Contact Angle of Water on Graphene?. Langmuir 2013;29:1457-65.
5   Xiong Z, Zhang L, Jizhen M, Zhao XS. Photocatalytic degradation of dyes over graphene–gold nanocomposites under visible light irradiation. Chem. Commun, 2010;46:6099-101.
6   Geng Z, Lin Y, Yu X, Shen Q, Zhaoyi LM, Pan N, Wang X. Highly efficient dye adsorption and removal: a functional hybrid of reduced graphene oxide–Fe$_3$O$_4$ nanoparticles as an easily regenerative adsorbent. J Mater Chem, 2012;22:3527-35.
7   Martinez-Orozco RD, Rosu HC, Lee SW, Rodríguez-González V. Understanding the adsorptive and photoactivity properties of Ag-graphene oxide nanocomposites. J Hazard Mater 2013;263:52-60.
8   Liu F, Chung S, Oh G, Seo TS, Three-Dimensional Graphene Oxide Nanostructure for Fast and Efficient Water-Soluble Dye Removal. Appl Mater Interfaces 2012;4:922-7.
9   Mani V, Chen SM, Lou BS. Three Dimensional Graphene Oxide-Carbon Nanotubes and Graphene-Carbon Nanotubes Hybrids. Int J Electrochem Sci 2013;8:11641-60.
10   Song LW, Lim SN, Kanga KK, Park SB. Graphene-based mesoporous nanocomposites of spherical shape with a 2-D layered structure. J Mater Chem A 2013;1:6719-22.
11   Wang T, Peng Z, Wang Y, Tang J, Zheng G. MnO nanoparticle@mesoporous carbon composites grown on conducting substrates featuring high-performance lithium-ion battery, supercapacitor and sensor. Sci Rep 2013;3:2693.
12   Liu J, Aksay LA, Kou R, Wang D. Mesoporous Metal Oxide Graphene Nanocomposite Materials. Patent US 20110051316 A1.
13   Liu Y, Jin H, Zhu S, Liu Y, Long M, Zhou Y, Yan D. A facile method for fabricating TiO2@mesoporous carbon and three-layered nanocomposites. Nanotechnology 2012;23:325602-8.
14   Wang D, Kou R, Choi D, Yang Z, Nie Z, Li J, Saraf LV, Hu D, Zhang J, Graff GL, Liu J, Pope MA, Aksay IA. Ternary Self-Assembly of Ordered Metal Oxide−Graphene Nanocomposites for Electrochemical Energy Storage ACS Nano, 2010;4:1587-95.
15   Ko JW, Kim S, Hong J, Ryu J, Kang K, Park CB. Synthesis of graphene-wrapped CuO hybrid materials by CO2 mineralization. Green Chem 2012;14:2391-4.

16   Marcano DC, Kosynkin DW, Berlin JM, Sinitskii A, Sun Z, Slesarev A, Alemany LB, Lu W, Tour JM. Improved Synthesis of Graphene Oxide. ACS Nano 2010;4:4806-14.

17   Liu X, Zhang H, Ma Y, Wu X, Meng L, Guo Y, Yu G , Liu Y. Graphene-coated silica as a highly efficient sorbent for residual organophosphorus pesticides in water. J Mater Chem A 2013;1:1875-84.

18   Fang X, Chen C, Liu Z, Liu P, Zheng N. A cationic surfactant assisted selective etching strategy to hollow mesoporous silica spheres. Nanoscale 2011;3:1632-9.

19   Song G, Li C, Hu J, Zou R, Xu K, Han L, Wang Q, Yang J, Chen Z, Qin Z, Ruan K, Hu R. A simple transformation from silica core–shell–shell to yolk–shell nanostructures: a useful platform for effective cell imaging and drug delivery. J Mater Chem 2012;22:17011-8.

20   Li Z, Barnes JC, Bosoy A, Stoddart JF, Zink JI. Mesoporous silica nanoparticles in biomedical applications. Chem Soc Rev 2012;41:2590-605.

21   Rath D, Parida KM. Copper and Nickel Modified MCM-41 An Efficient Catalyst for Hydrodehalogenation of Chlorobenzene at Room Temperature. Ind Eng Chem Res 2011;50:2839-49.

22   Wojtoniszak M, Zielinska B, Chen X, Kalenczuk RJ, Borowiak-Palen E. Synthesis and photocatalytic performance of TiO_2 nanospheres–graphene nanocomposite under visible and UV light irradiation. J Mater Sci 2012;47:3185-90.

23   Rasalingam S, Peng R, Koodali RT. An investigation into the effect of porosities on the adsorption of rhodamine B using titania–silica mixed oxide xerogels. J Environ Manag 2013;128:530-9.

24   Sharma P, Hussain N, Borah DJ, Das MR. Kinetics and Adsorption Behavior of the Methyl Blue at the Graphene Oxide/Reduced Graphene Oxide Nanosheet−Water. J Chem Eng Data 2013, 58, 3477-88.

25   Lee SY, Park SJ. Comprehensive review on synthesis and adsorption behaviors of graphene-based materials. Carbon Letters 2012;13:73-87.

26   Zubir NA, Yacou C, Motuzas J, Zhang X, Diniz da Costa JC. Structural and functional investigation of graphene oxide-Fe_3O_4 nanocomposites for the heterogeneous Fenton-like reaction. Sci Rep 2014:4:4594

27   Zhang J, Xiong Z, Zhao XS. Graphene-metal-oxide composites for the degradation of dyes under visible light irradiation. J Mater Chem 2011;21:3634-40.

28   Shang J, Ma L, Li J, Ai W, Yu T, Gurzadyan GG. The Origin of Fluorescence from Graphene Oxide. Sci Rep 2012;2:792.

29   Demchenko AP, Dekaliuk MO. Novel fluorescent carbonic nanomaterials for sensing and imaging. Methods Appl Fluoresc 2013, 1, 042001.

30   Wang Y, Chu W. Adsorption and Removal of a Xanthene Dye from Aqueous Solution Using Two Solid Wastes as Adsorbents. Ind Eng Chem Res 2011;50:8734-41.

31   Jevšnik S, Geršak J. Modelling a fused panel for a numerical simulation of drape. Fibres Text East Euro 2004;12:1:45-72.

32   Hussain SA, Banik S, Chakraborty S, Bhattacharjee D. Adsorption kinetics of a fluorescent dye in a long chain fatty acid matrix. Spectrochim Acta A, 2011;79:1642-7.

33   Li H, Zhang J, Zhou X, Lu G, Yin Z, Li G, Wu T, Boey F, Venkatraman SS, Zhang H. Aminosilane micropatterns on hydroxyl-terminated substrates: fabrication and applications Langmuir 2009;26:5603-9.

List of figures

Fig. 1. a) XRD patterns showing the structural evolution; b) FTIR spectra of the main functional groups; c) N_2 isotherms; and d) pore size distribution.

Fig. 2. a), b) TEM images of GO-SNS; c) Mesoporous SNS HRTEM showing hexagonal arrangement; d) Histogram of average particle size of SNS.

Fig. 3. Effect of RhB adsorption as a function of time: a) 5 ppm, b) 10 ppm of RhB, c) RhB reduction using hydrazine and d) UV-vis spectra after RhB adsorption.

Highlights

SiO$_2$/GO assembly are synthesized by the one-step hydrothermal technique.

The assembly has strong RhB adsorption capacity, which fits with the Langmuir model.

The reduction activity using N$_2$H$_2$ as a sacrificial electron donor was 50% of RhB.

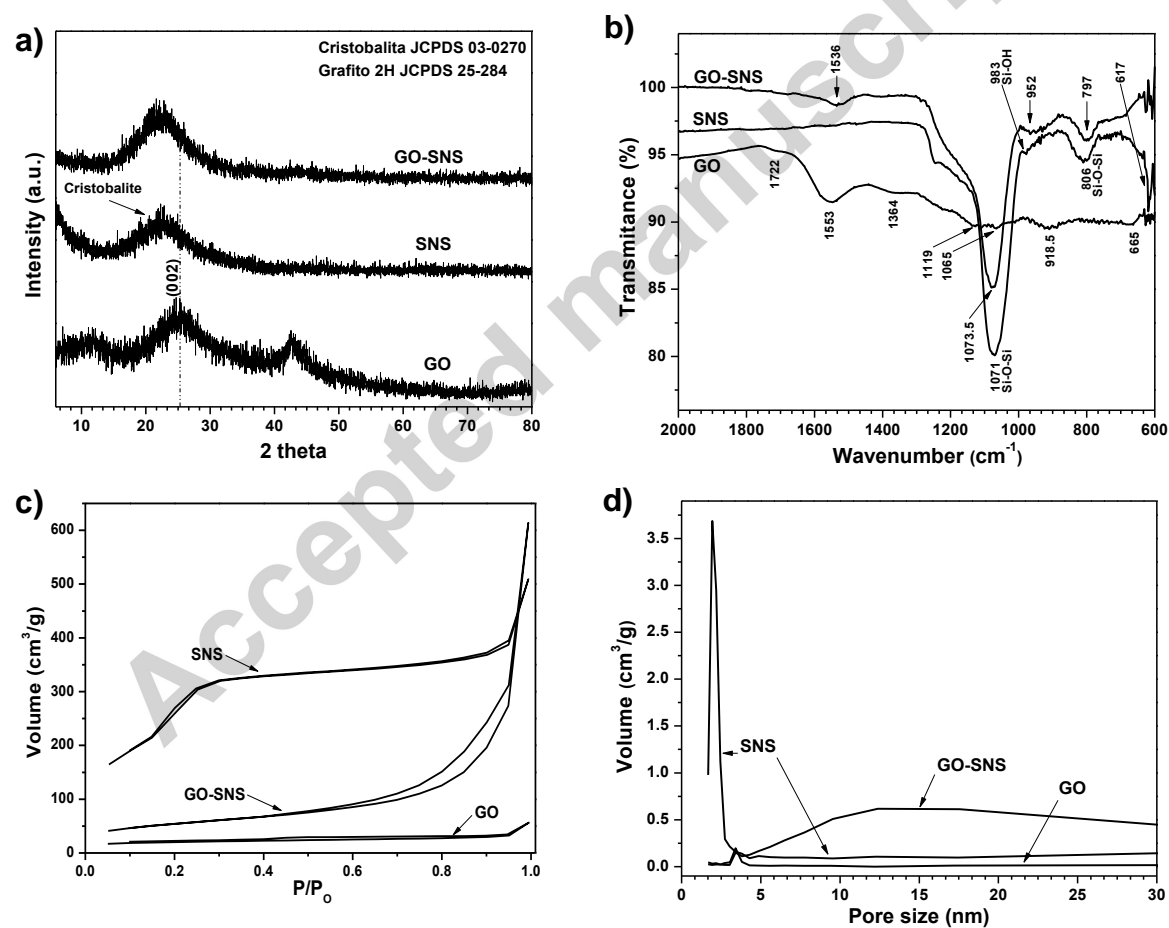The assembly stained by RhB can be used in high visibility paint products.
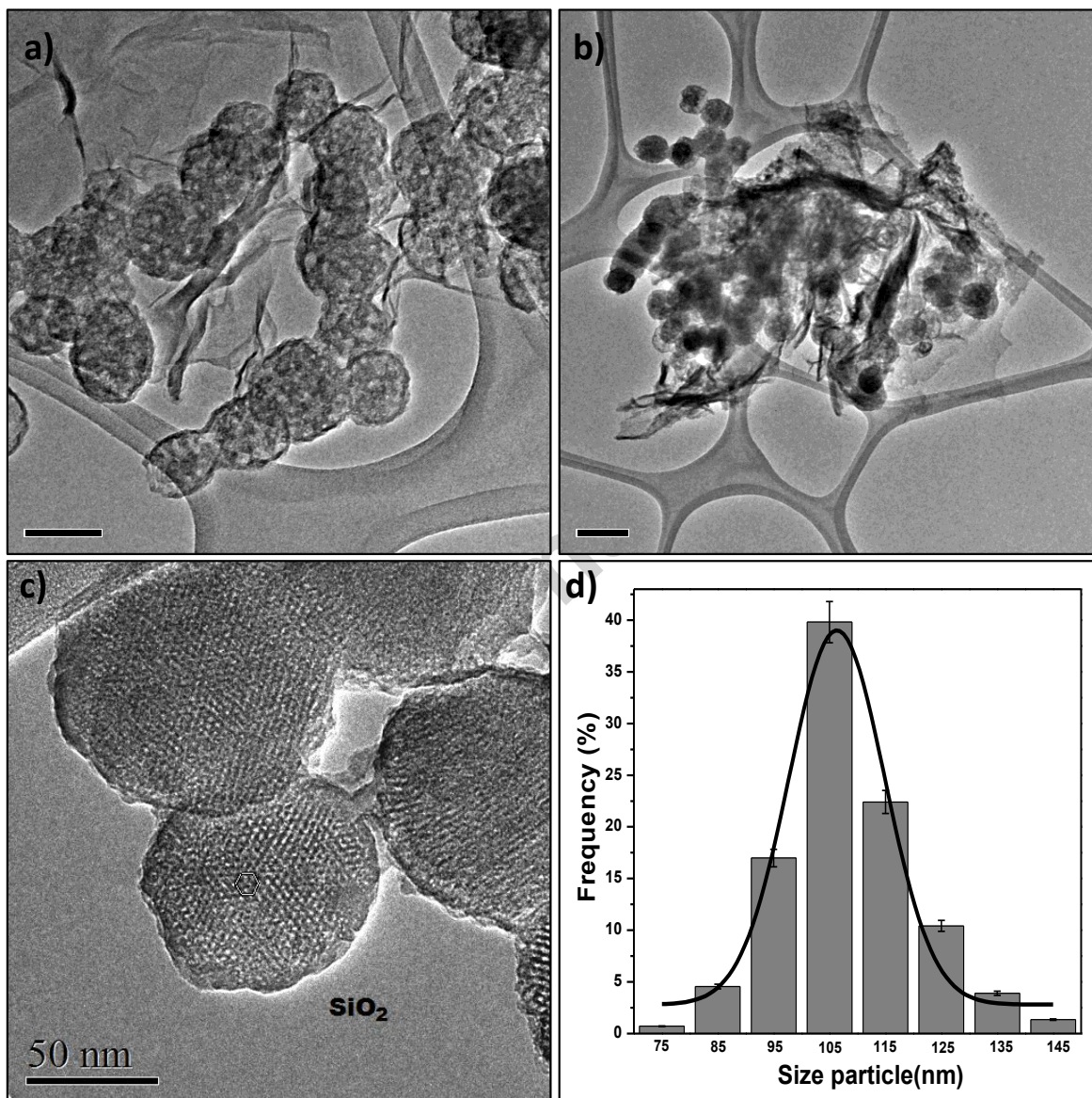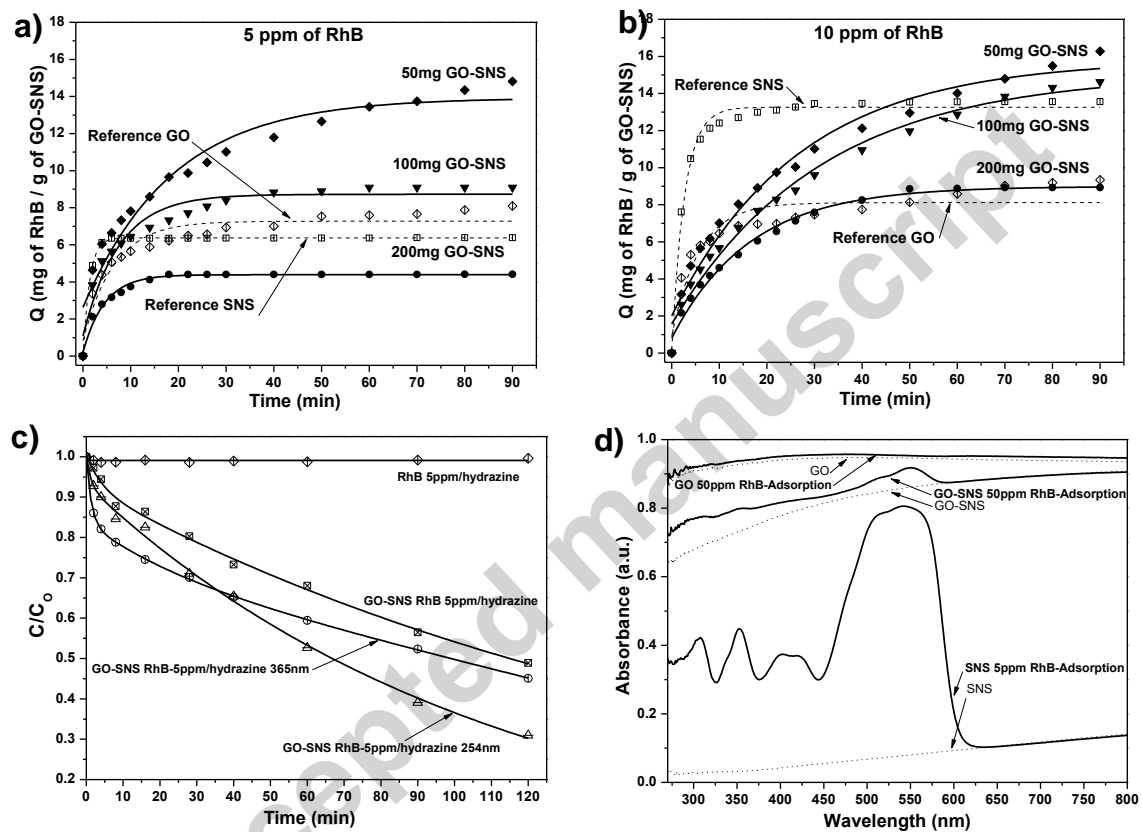
Figure 1

Figure 2

Figure 3

A functional assembly of SiO$_2$ nanospheres/Graphene Oxide composites.

J. Iturbe-Ek[1], J. Andrade-Martínez[1, 2], R. Gómez[3] and V. Rodríguez-González*[1]

[1]*División de Materiales Avanzados, Instituto Potosino de Investigación Científica y Tecnológica, Camino a la Presa San José 2055 Col. Lomas 4a. sección C.P. 78216, San Luis Potosí, S.L.P., México.*

[2]*Doctorado Institucional en Ingeniería y Ciencia de Materiales, Universidad Autónoma de San Luis Potosí, Av. Manuel Nava No. 6, Zona Universitaria, San Luis Potosí, SLP, México*

[3]*Departamento de Química, ECOCATAL, Universidad Autónoma Metropolitana-Iztapalapa, México, D.F., 09340, México*

14